Astron. Astrophys. 328, 606–616 (1997)

ASTRONOMY AND ASTROPHYSICS

Nitrogen V in the wind of the pre-main sequence Herbig Ae star AB Aurigae⋆

J.-C. Bouret[1], **C. Catala**[1], **and T. Simon**[2]

[1] Laboratoire d'Astrophysique de Toulouse, CNRS UMR 5572, Observatoire Midi-Pyrénées, 14, Avenue Edouard Belin, F-31400 Toulouse, France

[2] Institute for Astronomy, University of Hawaii, 2680 Woodlawn Drive, Honolulu, Hawaii 96822, USA

Received 12 May 1997 / Accepted 5 August 1997

Abstract. Recent GHRS observations of the Herbig Ae star AB Aur demonstrate the presence of N V in the wind of this star. This result reveals temperatures much higher than those previously considered for the wind of AB Aur. We show that homogeneous spherically symmetric models are unable to reproduce the available observations, including the C IV resonance lines in absorption and the absence of N IV emission. We then study models including hot (T≈140,000 K) clumps, and argue that the N V lines can be formed in such hot regions. The filling factor of the hot clumps can be as small as a few 10^{-3}. This type of clumpy structure of the wind is expected in the framework of a model of the wind of AB Aur, in which fast and slow streams alternate, and produce shocks where fast streams overtake slow ones. The presence of shocks in the wind of AB Aur would also be consistent with its X-ray emission.

Key words: line: profiles – stars: AB Aur – stars: chromospheres – stars: pre-main sequence – stars: mass loss

1. Introduction

The class of the Ae/Be Herbig stars was defined by Herbig in 1960, as a group of stars of spectral types earlier than F0 with emission lines, embedded in dense molecular clouds, and illuminating bright reflection nebulae. More than thirty years later, the pre-main sequence nature of these stars is now well established (Strom et al. 1972; Finkenzeller & Jankovics 1984). According to the standard theory of stellar evolution, pre-main sequence stars with intermediate masses (2-5 $M_{\odot}$) do not have outer convection zones. Since stellar activity is generally considered to be linked to the existence of such convection zones which give rise to magnetic fields or acoustic waves, activity manifestations are unexpected in Herbig stars. However, strong evidence for activity and stellar winds have been observed for most of them. The resonance lines of Si IV and C IV (Catala et al. 1984), or emission in Mg II h and k, He I 5876Å, etc., are clues for the existence of heated layers in the outer atmosphere of these stars, while P Cygni profiles of Mg II h and k and of hydrogen Balmer lines are characteristic of stellar winds.

Among the Herbig Ae stars, AB Aurigae (A0Ve) is usually considered as the prototype of the whole class. All the wind and activity signatures listed above are observed in its spectrum (Böhm & Catala 1993 and 1994; Catala et al. 1993). A model of its wind, including an extended chromosphere, has been developed, to account for the spectral features that are observed (Catala et al. 1984; Catala & Kunasz 1987; Catala 1988). Constraints on the structure of the wind have been deduced from the studies of the C IV resonance lines seen in absorption, and the P Cygni profile of Mg II h and k and Hα. The chromosphere was found to be extended over $1.5R_*$ and its maximum temperature to be 17000K. A mass loss rate of the order of 10^{-8} $M_{\odot}$ yr^{-1} was also derived from this model. The radiative losses due to the chromosphere have been evaluated by Catala (1989), who found a total amount of several percent of the bolometric luminosity of the star. The major contribution to these radiative losses comes from the Balmer continuum, accounting for more than half of them.

Observations performed with ROSAT (Zinnecker & Preibisch 1994) have shown that among a sample of 21 Herbig stars, 11 of them exhibit X-ray emission. AB Aur is one of these stars, with L_X/L_{bol}=1.6×10^{-6}. Several scenarios have been developed to explain the origin of this emission, some of them suggesting the presence of unresolved T Tauri companions around the Herbig stars, or the existence of a disk corona. However the existence in the wind of layers heated to temperatures much higher (T≥ 10^6K) than those previously supposed is often considered; the location of these layers and the heat-

Send offprint requests to: J.-C. Bouret (bouret@astro.obs-mip.fr)

⋆ Based on observations with the NASA/ESA *Hubble Space Telescope (HST)*, which is operated by the Space Telescope Science Institute under NASA contract NAS5-26555 to the Association of Universities for Research in Astronomy, Inc, and on observations made by the International Ultraviolet Explorer (IUE) and collected at the Villafranca Satellite Tracking Station of the European Space Agency.

ing mechanism are still unknown, but this hypothesis seems to be the most convincing cause for the X-ray emission. With respect to this last point, the presence of such heated zones could also induce the formation of species like O VI or N V since high temperatures are required to form such ionization stages, even if these species can be formed with lower temperatures than those needed to produce X-rays (Catala 1984; Catala & Kunasz 1987).

In the last years, many observations of rotational modulation for several lines of the spectrum of AB Aur have been accumulated (Böhm et al. 1996), leading to the conclusion that azimuthal structures are present in the wind of this star, which are interpreted as the alternation on the line of sight of fast and slow streams, probably linked to the existence of a magnetic field. Due to the strong difference of velocities of the two sorts of streams, shocks are expected to form where the fast streams overtake slow ones, leading to a strong increase of the local temperature, probably high enough to produce the aforementioned species, as well as the X-ray emission. This idea is strengthened by the fact that Donati et al. (1997) have recently obtained the first direct clue of the existence of a magnetic field in Herbig stars, thanks to polarimetric observations of the star HD 104237 (spectral type A4V).

In Sect. 2 we describe the observation of N V and C IV resonance lines by HST. Sect. 3 presents the wind and atomic models that have been used in this work, as well as a summary of the method used to solve the transfer equation. Results and their significance are discussed in section IV, and a conclusion is given in Sect. 5.

2. Observations and data reduction

2.1. HST observations

AB Aur was observed at intermediate spectral resolution with the Goddard High Resolution Spectrograph (GHRS) aboard the Hubble Space Telescope (HST) on 1996 February 23. Two spectral regions were observed, the 1536–1563 Å region surrounding the C IV doublet at 1548.2, 1550.8 Å (dataset Z33W0104T), and the 1226–1253 Å region which is centered on the N V doublet at 1238.8, 1242.8 Å (dataset Z33W0105T). The observations were acquired with the G140M grating and through the large science aperture. The integration times were 980 seconds at C IV and and 6093 seconds at N V, respectively. In both cases, we followed the standard observing procedures, as described in the GHRS *Instrument Handbook* (Soderblom et al. 1995). These include sub-stepping the spectrum by fractional diodes of the Digicon detector for better sampling, moving the spectrum by integral numbers of diodes to correct for diode defects, and multiple-diode rotations of the grating to help remove the fixed pattern noise. The wavelength scales were verified and adjusted according to the SPYBAL calibration spectrum that accompanies each science observation (see Soderblom et al. 1995); corrections of -0.052 Å were made to the zero-points of the wavelength scales at both N V and C IV. In addition to the correction on the wavelength scale due to the instrumental drift in zero-point, we also corrected it for the radial velocity of the star (+21 km.s^{-1}).

Table 1. Atomic transitions giving rise to the lines observed on the HST spectrum.

Wavelength	Species	Transition
1238.8	N V	2s $^2S_{1/2}$ - 2p $^2P_{3/2}$
1240.4	Mg II	3s $^2S_{1/2}$ - 4p $^2P_{3/2}$
1242.8	N V	2s $^2S_{1/2}$ - 2p $^2P_{1/2}$
1243.2	N I	$2p^3$ $^2D^o_{5/2}$ - $2p^2$3s $^2D_{5/2}$
1243.3	N I	$2p^3$ $^2D^o_{3/2}$ - $2p^2$3s $^2D_{3/2}$
1249.8	P II	$3p^2$ $^1D_2$ - 3p4s $^1P^0_1$
1249.9	Mg II	3p $^2P^0_{3/2}$ - 10s $^2S_{1/2}$
1250.1	Si II	3s$3p^2$ $^2D_{3/2}$ - $3p^3$ $^2D^0_{3/2}$
1250.5	S II	$3s^2$$3p^3$ $^4S^0_{3/2}$ - 3s$3p^4$ $^4P_{1/2}$
1253.3	S I	$3p^4$ $^3P_1$ - $3p^3(^4S^0)6d$ $^3D^0_2$

2.2. The line profiles

The data supplied by the standard pipeline processing of HST were analyzed within STSDAS/IRAF. Fig. 1 shows the spectrum in the region of the C IV resonance lines. As observed repeatedly in the past (Catala & Talavera 1984; Catala et al. 1987), the C IV resonance doublet appears purely in absorption. The lines are broad, asymmetric, with a clear extension toward the blue, indicating that they are formed in the wind. The violet edge of the lines corresponds to a velocity of about -260 km.s^{-1}, a value similar to that obtained by Catala & Talavera (1984).

Fig. 2 shows the observed spectrum in the wavelength region of the N V resonance doublet. In order to ascertain the presence of N V lines in the spectrum presented in Fig. 2, we have identified all the features appearing in this spectrum, thanks to Kurucz's synthetic spectrum for T_{eff} = 10000K and log(g)=4, adequate for AB Aur (Böhm & Catala 1993). Table 1 lists the atomic transitions responsible for the lines. The deep absorption (almost saturated) at $\lambda \sim 1242.5$Å is most likely the blueshifted absorption component of a PCygni profile for the N I multiplet 5 lines. We have checked on IUE spectra that the multiplet 4 of N I is present, strengthening this identification. These lines are presented in Fig. 3. Both lines of N I multiplet 4 are blueshifted and purely in absorption. The violet edge of the line at 1492.6Å is $\Delta V \sim 203$ km.s^{-1}, while that of the line at 1494.6Å is $\Delta V \sim 193$ km.s^{-1}. These values are to be compared with the one found for the absorption component of the P Cygni profile mentioned above, which is $\Delta V \sim 277$ km.s^{-1}. It is likely that all these lines are formed in the wind, but since the multiplet 5 lines are formed in a region where the continuum is weaker, they appear more easily with a P Cygni profile. The discrepancy between the blueshifts of the absorption troughs of these two multiplets is not surprising since the corresponding spectra have been obtained at different dates, and since the velocity in the wind of AB Aur is known to vary significantly with time (Praderie et al. 1986).

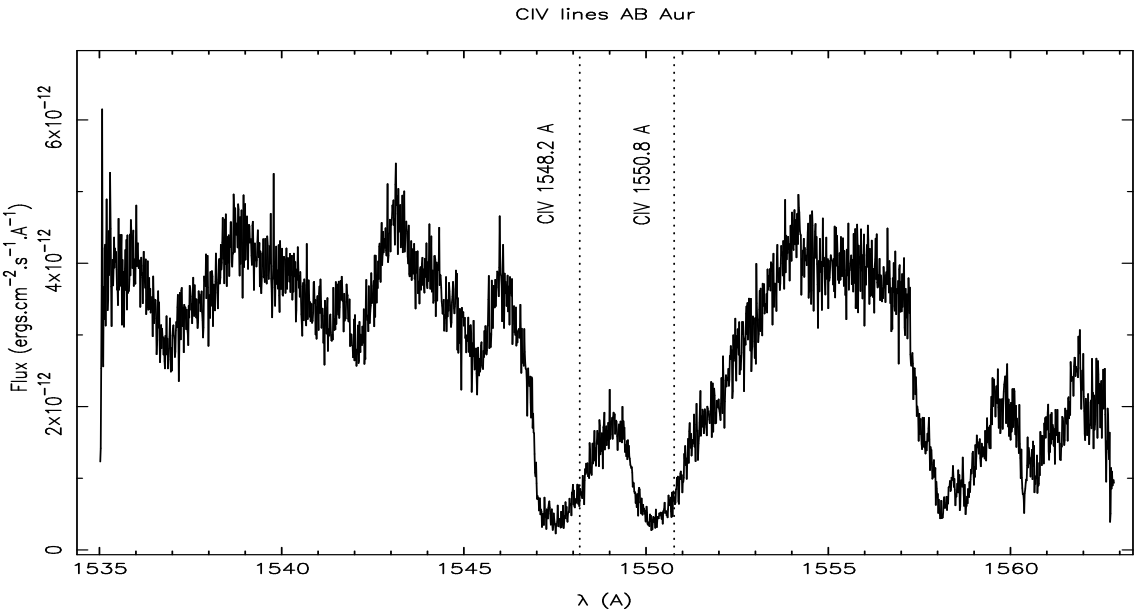

Fig. 1. Observed spectrum of AB Aur, obtained with GHRS spectrograph of HST, the region of the C IV resonance doublet.

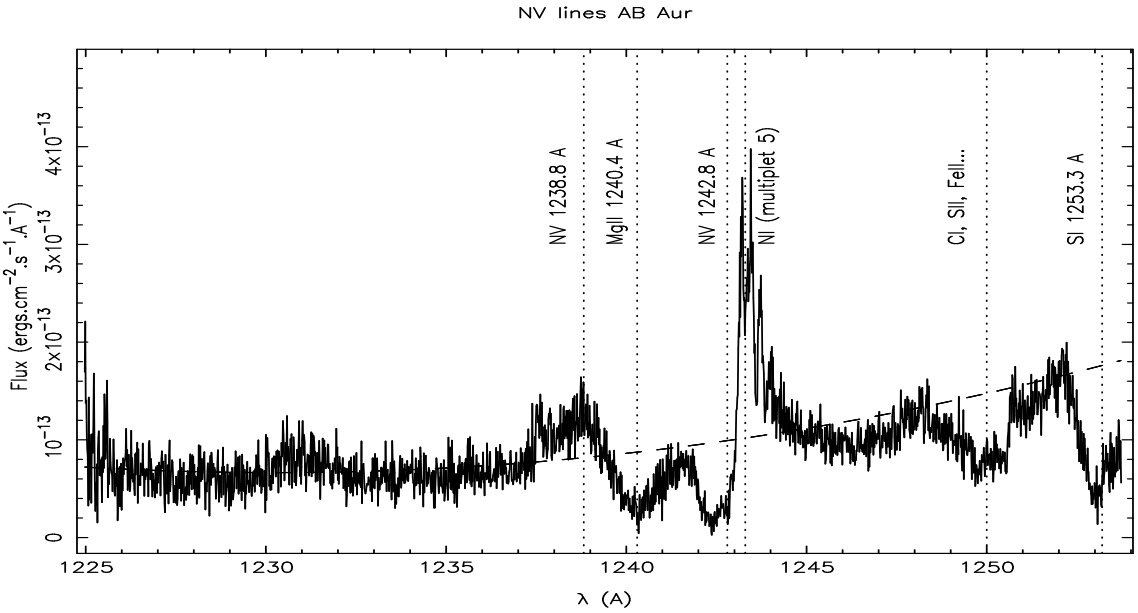

Fig. 2. Observed spectrum of AB Aur, obtained with GHRS spectrograph of HST, in the spectral region of the N V resonance doublet. The dashed line represents the continuum used to normalize the spectrum. Vertical dotted lines indicate the lines identified in the spectrum.

A particular attention was given to the absorption feature at 1240.4 Å, which could be falsely interpreted as the absorption component of an inverse P Cygni profile of N V. We have checked that it is in fact the 3s-4p resonance line of Mg II. We have calculated this line with the ETLA code (see below) in the frame of the photosphere-chromosphere-wind model of Catala & Kunasz (1987), and have found that it is purely photospheric, and appears in absorption in the synthetic spectrum, centered at the rest wavelength. Since the stellar rotation influences the shape of this line, we have convolved the profile produced by ETLA with the rotational profile of AB Aur (vsini=80 km.s^{-1}; Böhm & Catala 1993). Since the final synthetic profile fits reasonably well the observed one, we conclude that this feature in the HST spectrum can be identified as the 3s-4p resonance line of Mg II.

We identified the emission feature detected at $\lambda \sim 1238.8$Å as one component of the 2s-2p resonance doublet of N V. We should therefore in principle see the other component of this doublet at $\lambda \sim 1242.8$Å. Unfortunately, this second component is totally blended with the absorption component of the N I

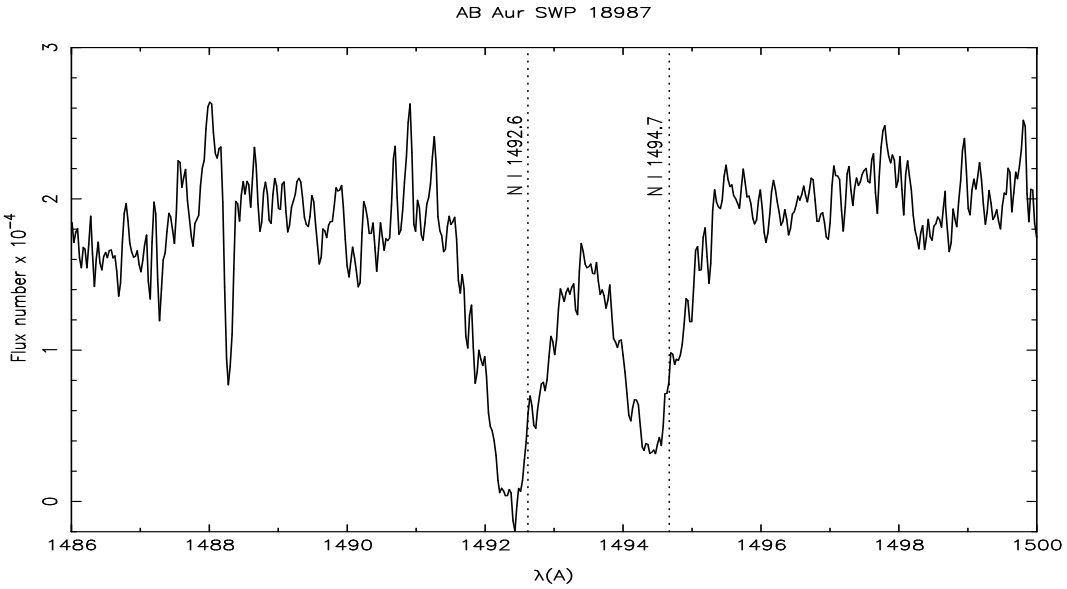

Fig. 3. IUE spectrum of AB Aur, in the region of N I multiplet 4. The wavelength scale was set with respect to the interstellar line of C I at 1656.93 Å, also present in the IUE spectrum.

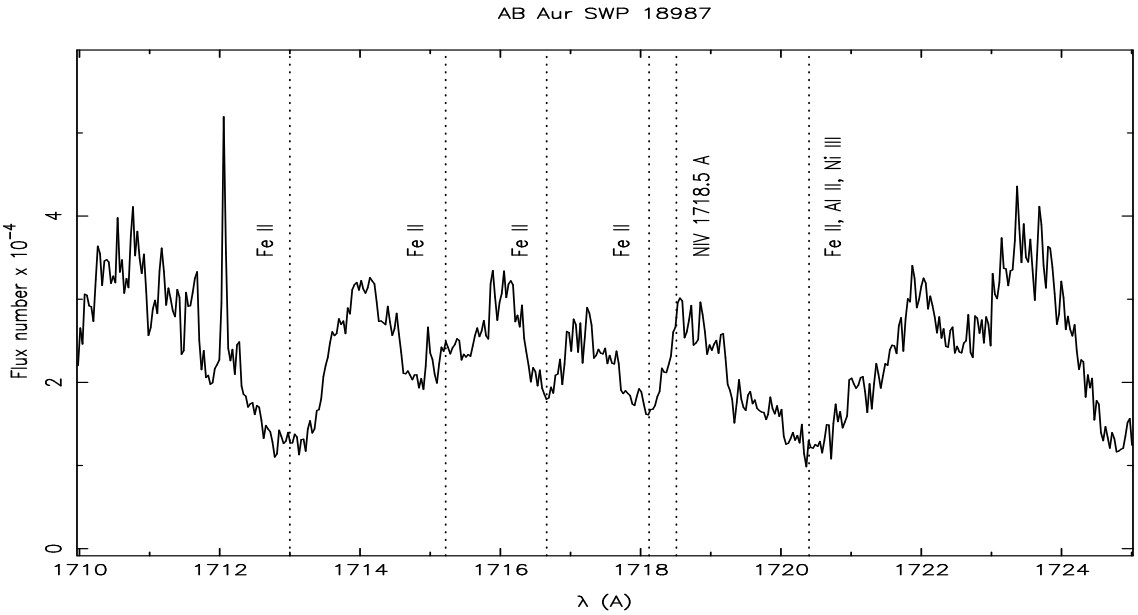

Fig. 4. IUE spectrum of AB Aur, in the region of N IV multiplet 7. The wavelength scale was set with respect to the interstellar line of C I at 1656.93 Å, also present in the IUE spectrum.

lines of multiplet 5. A very weak emission seen at this wavelength probably corresponds to this second line of the resonance doublet of N V. We thus conclude that the resonance doublet of N V is present in the GHRS spectrum of AB Aur.

Finally, we have searched IUE spectra of AB Aur for the N IV line at 1718.51 Å (multiplet 7), and our own archive of MUSICOS spectra for the N IV line at 7651.4 Å. Neither of these two lines was detected. Fig. 4 shows the IUE spectrum on the region of the N IV line at 1718.51 Å. Clearly, no conspicuous line is seen at 1718.51 Å. The other lines of this spectrum have been identified thanks to the atomic data table of Kelly & Palumbo (1973); in addition, our identifications have been strengthened by comparison with the spectral atlas of the normal B star ν Capricorni (spectral type B 9.5) elaborated by Artru et al. (1989).

We thus conclude that the ionization balance of nitrogen is shifted toward higher ionization stages in the region of the

wind producing the N V resonance lines, which will constitute a powerful constraint on the models presented below.

3. Formation of N V lines

3.1. The atmospheric model

The presence of N V resonance lines indicates temperatures much above those of the current model of AB Aur's wind (Catala & Kunasz 1987, hereafter CK), which includes a maximum temperature of 17000K in the chromosphere. We therefore need to introduce an additional high temperature zone (hereafter HTZ) in the model of CK. In the following of this paper, we first consider a spherically symmetric model, then departures from spherical symmetry inspired from the azimuthal structures in the wind witnessed by the rotational modulation detected in some lines of AB Aur (Praderie et al. 1986; Catala et al. 1986). Although the basic model is fully described in CK, we recall here some of its principal properties.

We use a non-rotating and spherically expanding model of stellar wind. All the variables used in the model are functions of the radial distance r from the center of the star. At the base of the wind, we put a classical photosphere (Kurucz) in radiative and hydrostatic equilibrium; the temperature in the photosphere decreases outward, until it reaches a minimum value $T_{min} < T_{eff}$.

The velocity law of the expanding atmosphere is monotonically increasing outward, and is given as a linear function of r. The density is determined through the equation of continuity, by using the velocity law and the assumed value of $\dot{M}$. In addition to this expansion velocity field, we assumed the existence of macroscopic turbulent motion in the wind. We have taken it into account by means of a free parameter, v_D , considered as a Doppler random velocity. This parameter acts as a non thermal broadening component in the intrinsic line profile.

The difference between the "classical" model of CK, and the present one, is the temperature law in the expanding wind. In the model of CK, which includes only a moderate temperature chromosphere, the temperature law is governed by four parameters,T_{max}, Δ_1,Δ_2,T_0:

$$T(r) = \begin{cases} T_0 + (T_{max} - T_0) exp\left[-4ln2\frac{(r-R_{ch})^2}{\Delta_1^2}\right] \\ \text{if } R_{ph} \leq r \leq R_{ch} \\ T_0 + (T_{max} - T_0) exp\left[-4ln2\frac{(r-R_{ch})^2}{\Delta_2^2}\right] \\ \text{if } R_{ch} < r \end{cases} \quad (1)$$

the maximum temperature T_{max} being reached in the chromosphere at the point R_{ch} given by:

$$R_{ch} = R_{ph} + \frac{\Delta_1}{2(ln2)^{1/2}} \left[ln\left(\frac{T_{max} - T_0}{T_{eff} - T_0}\right)\right]^{1/2} \quad (2)$$

where R_{ph} is the photospheric radius. Δ_1 and Δ_2 control respectively the position of the maximum temperature, and the chromospheric extension, while T_0 is the temperature of the cool region in the external part of the wind. All these parameters have been tightly constrained by CK on the basis of Mg II, Hα, and C IV and we considered them fixed; we recall briefly the values they found: Δ_1 = 0.08 R_{ph}, Δ_2 = 1.5 R_{ph}, T_{max}=17000K, T_0=3000K, v_D =45 km.s^{-1}. Furthermore, we used the mass loss rate $\dot{M}$= 1.1 $\times 10^{-8}$ $M_\odot yr^{-1}$ and the velocity law of their best fit model.

In the present model, we introduce an additional HTZ, controlled by three parameters (Δ_3,Δ_4, T_{htz}), which describe respectively the position, the width, and the temperature of the HTZ. The maximum temperature in this region T_{htz} is reached at a radial distance from the center of the star, given by

$$R_{htz} = R_{ph} + \Delta_3 \quad (3)$$

Parameter Δ_4 describes the width of the HTZ; the HTZ extends from $R_1 = R_{htz} - \Delta_4$ to $R_2 = R_{htz} + \Delta_4$. The temperature law in the HTZ is then given by:

$$T(r) = \begin{cases} T(R_1) + (T_{htz} - T(R_1)) exp\left[-4ln2\frac{(r-R_{htz})^2}{\Delta_4^2}\right] \\ if\ R_1 \leq r \leq R_{htz} \\ T(R_2) + (T_{htz} - T(R_2)) exp\left[-4ln2\frac{(r-R_{htz})^2}{\Delta_4^2}\right] \\ if\ R_{htz} \leq r \leq R_2 \end{cases} \quad (4)$$

where T(R_1) and T(R_2) are the temperatures of the CK model at distances R_1 and R_2, respectively.

3.2. Atomic model

In this work, we have considered three ionization states, N IV, N V, N VI, and for each of them a different number of levels: 5 for N IV, 2 for N V, 1 for N VI. Although the number of levels considered for N V is low, it is sufficient for the accuracy we want to reach. We only consider the first two levels of N V (2s $^2S_{1/2}$, 2p $^2P^0_{1/2}$) because they are well decoupled from the other levels of the ion. Such an atomic model involves 18 transitions: 11 bound-bound transitions and 7 bound-free transitions. The atomic fine structure was ignored, except for the resonance line of N V we are studying. In this case, we have considered that LTE balance is achieved between the sub-levels, and that there is no difference of energy between them. From the statistical equilibrium equations we obtain the values of n_{nl}, the population of each (*n,l*) state summed over all *j* -states. The individual components are then calculated by:

$$n_{nlj} = \frac{(2j+1)}{2(2l+1)} n_{nl} \quad (5)$$

For all the lines, except the N V resonance lines, intrinsic profiles have been assumed Gaussian, with widths calculated from the Doppler random velocity given in the wind model. For the N V resonance lines, we have used a Voigt profile, with a damping parameter a estimated from Sahal-Brechot et al. (1971); since a is dominated by radiative damping, which does not depend on electron density, it has been taken constant over the wind, with a value of 2 $\times 10^{-4}$.

Collisional excitation and ionization rates as well as some photo-ionization cross-sections have been calculated from data

Table 2. Atomic parameters, E is the energy level and E_i is the ionization energy from this level

No.	Level	Stat. weight	E(cm^{-1})	$E_i(cm^{-1})$
1	N IV $2s^2\ ^1S$	1	0	624851.0
2	N IV 2s 2p $^3P^0$	9	67226.6	557624.4
3	N IV 2s 2p $^1P^0$	3	130695.0	494156.0
4	N IV 2p 2p ^3P	9	173553.9	449297.1
5	N IV 2p 2p ^1D	5	188885.0	435966.0
6	N V 2s $^2S_{1/2}$	2	624851.0	789532.9
7	N V 2p ^2P	6	705445.1	333398.9
8	N VI $1s^2\ ^1S$	1	1414383.9	0

Table 3. Oscillator strengths

Transition	f
N IV $2s^2\ ^1S$ - N IV 2s 2p $^3P^0$	5.500 10^{-7}
N IV $2s^2\ ^1S$ - N IV 2s 2p $^1P^0$	0.620
N IV $2s^2\ ^1S$ - N IV 2p 2p ^3P	1.000 10^{-13}
N IV $2s^2\ ^1S$ - N IV 2p 2p ^1D	1.000 10^{-13}
N IV 2s 2p $^3P^0$ - N IV 2s 2p $^1P^0$	1.000 10^{-13}
N IV 2s 2p $^3P^0$ - N IV 2p 2p ^3P	1.000 10^{-13}
N IV 2s 2p $^3P^0$ - N IV 2p 2p ^1D	6.400 10^{-4}
N IV 2s 2p $^1P^0$ - N IV 2p 2p ^3P	2.830 10^{-5}
N IV 2s 2p $^1P^0$ - N IV 2p 2p ^1D	0.173
N IV 2p 2p ^3P - N IV 2p 2p ^1D	1.000 10^{-13}
N V 2s $^2S_{1/2}$ - N V 2p ^2P	0.213

and formulae found in Hubeny's TLUSTY code (Hubeny, private communication): for most of the collisional ionizations, the relations are those of Seaton (1962), while the collisional excitations are treated through the Van Regemorter (1962) formula; the photo-ionizations rates calculations are mostly based on the quantum defect method of Peach (1967). For those of the photo-ionization cross-sections that have not been evaluated with the aforementioned data, we have used data provided by Hidalgo (1968).

Following Catala (1988), we have neglected auto-ionization and dielectronic recombinations, and we have assumed complete redistribution. Finally, we have adopted a nitrogen abundance of 1.12 10^{-4}. All the atomic parameters used here are given in table 2 and table 3.

3.3. Solution of the transfer equation

For the solution of the transfer equation, we have used the method of the equivalent two-level atom (ETLA) in the comoving frame, introduced by Mihalas et al. (1978). A discussion of the use of ETLA in the problem of winds of Herbig Ae/Be stars has been given in CK. We just recall here some important points of this method.

The first step of ETLA is to solve the transfer equation together with the equations of statistical equilibrium, in the comoving frame formulation. Once this step has been performed, calculations in the observer's frame give the emergent flux, which can be directly compared to observations. Background opacity and emissivity sources are set in LTE, with normal abundances. They include 10 levels for H, 20 levels for He, and a total of 24 levels for C, N, O, Ne, Si and their ions.

The fine structure of the N V resonance doublet was taken into account, which allowed us to compute the bluest line separately.

In a first stage the Doppler random velocity was set to the value found by CK, i.e., 45 km.s^{-1}, then we introduced higher values to improve the fit of the observed line by the synthetic profile (see discussion below).

For models with departures from spherical symmetry, we have first solved the transfer equation in the comoving frame with our spherically symmetric model, and derived the opacities and source functions in spherical symmetry. In a second step, we have calculated the emergent intensity over an arbitrary geometry in the observer's frame, using the source functions computed with the spherically symmetric model.

More precisely, the presence of shocks, producing hot clumps of material in the wind, was simulated by a two-step procedure. First, we built a spherically symmetric model including a geometrically thin shell of high temperature, with a very steep temperature gradient at its inner and outer boundaries. The radiative transfer and statistical equilibrium equations were solved simultaneously for this model, yielding the source functions. Second we calculated the emergent intensity on a set of rays parallel to the line of sight from the observer, in the usual manner (see CK for details). The emergent flux was then computed by integrating the emergent intensity on the different rays, but we introduced the departures from spherical symmetry by weighting this integration by a function $r(\theta, \phi)$, representing the distribution of shocks in the wind. The assumption behind this procedure is that N V is present only in the hot clumps produced by the shocks, so that its opacity is non-zero only on rays that intercept hot clumps. The final integration of the emergent intensity into the emergent flux can thus be written as:

$$F(\nu) = \int_0^{2\pi} d\phi \int_{-\pi/2}^{\pi/2} cos\theta \,[r(\theta,\phi)I(\nu,\theta) + [1 - r(\theta,\phi)]\, I(\nu_c,\theta)]\, d\theta \tag{6}$$

If we assume that the dependence of $r(\theta, \phi)$ can be written as

$$r(\theta,\phi) = r_1(\phi) r_2(\theta) \tag{7}$$

i.e., that the distributions of hot clumps in latitude and longitude are uncorrelated, the expression of $F(\nu)$ becomes:

$$F(\nu) = 2\pi f_\phi \int_{-\pi/2}^{\pi/2} cos\theta\, r_2(\theta)\, [I(\nu,\theta) - I(\nu_c,\theta)]\, d\theta + 2\pi \int_{-\pi/2}^{\pi/2} cos\theta\, I(\nu_c,\theta) d\theta \tag{8}$$

where

$$2\pi f_\phi = \int_0^{2\pi} r_1(\phi)\, d\phi \tag{9}$$

In our models, $r_1(\phi)$ is assumed random, so that we just have to specify an azimuthal filling factor f_ϕ, while $r_2(\theta)$ is specifically given. We chose to define $r_2(\theta) = a(\theta)cos\theta$, where $a(\theta) = a_1$ for the rays that hit the stellar photosphere, and $a(\theta) = a_2$ for rays that do not. In this way, hot clump distributions more or less crowded near the equator can be simulated. The resulting total filling factor is thus:

$$f = \frac{f_\phi}{\pi} \int_{-\pi/2}^{\pi/2} r_2(\theta)\, d\theta \tag{10}$$

As far as the 1548.2 Å CIV line is concerned, the method used to calculate the N V line no longer applies. Indeed, Catala (1988) has shown that this line appears even if the temperature in the wind is about 17000K. Therefore, it is not possible to consider that the opacity in the line is zero everywhere except in the HTZ, nor that the emergent flux can be calculated with the method introduced hereabove.

We proceeded as follow: the contribution of the HTZ to the emergent specific intensity ($I^1(\nu,\theta)$) has been evaluated by subtracting the emergent specific intensity given by the classical model without the HTZ ($I^0(\nu,\theta)$) from the homogeneous model with the HTZ. Then, clumpiness was introduced when calculating the emergent flux:

$$F(\nu) =$$

$$\int_0^{2\pi} d\phi \int_{-\pi/2}^{\pi/2} cos\theta \left[r(\theta,\phi) I^1(\nu,\theta) + [1 - r(\theta,\phi)]\, I^1(\nu_c,\theta)\right] d\theta$$

$$+ \int_0^{2\pi} d\phi \int_{-\pi/2}^{\pi/2} cos\theta\, I^0(\nu,\theta)\, d\theta \tag{11}$$

4. Discussion

4.1. Spherically symmetric models with a high temperature zone

The profile of the N V resonance line depends critically upon the location of the HTZ. If the HTZ is close to the photosphere we obtain a single peak emission profile; models involving an HTZ more and more distant from the photosphere produce a double-peak emission profile, with a central absorption deeper as the HTZ gets closer to the top of the chromosphere. The interpretation of the evolution of the emission profile with the position of the HTZ in the velocity field is as follows.

Close to the photosphere, the velocity is small and the density is high so that a geometrically thin HTZ, with temperatures of the order of 60,000 K, is sufficient to reproduce the observed N V line. In spite of the relatively high density in this region, the HTZ is optically thin. The broadening due to the velocity field is small, and in all cases smaller than the Doppler width of the line. On rays that do not hit the stellar surface, two components are formed, one from the part of the HTZ moving toward us (with negative projected velocity), the other from the part of the HTZ moving away from us. They are obviously in emission since they are formed on no background continuum. Because of the low velocity in this part of the wind, the separation between these two components is smaller than the width of the line (natural width + thermal width). After integration on impact parameters, a single emission peak is obtained, as observed. These kinds of spherically symmetric models are thus consistent with the observed N V line. However, they produce a strong emission in the N IV 1718.51 Å line, which is not observed. This is due to the relatively low temperature of the HTZ, in which the ionization balance of nitrogen is strongly biased toward N IV. These models must therefore be discarded.

As the HTZ moves away from the photosphere and approaches the top of the chromosphere, its size must increase together with its maximum temperature, to produce enough N V to form the observed line. Temperatures of the order of 90,000 K are now necessary. On the central rays, the line appears in absorption, while on the rays that do not hit the stellar surface, two well-separated emission components appear, since the velocity in these regions is larger than the line width. The profile resulting from integration on impact parameters is thus a double-peak emission profile. Whether the central depression is under the continuum level or not, depends on the distance of the HTZ to the photosphere: the farther out the HTZ, the deeper the absorption component formed on central rays. It is therefore more and more difficult to fill it in with the emission components originating from rays that do not hit the stellar surface. These models cannot reproduce the observed N V line. In addition, they also produce an emission in the N IV 1718.51 Å line, and thus must be discarded as well.

When the HTZ is located far away in the wind, above the top of the chromosphere, in regions where the density is low, temperatures ranging from 10^5K to 2×10^5K are necessary to form an appreciable spectral feature.

When very close to the top of the chromosphere, a narrow HTZ is sufficient to produce an emission line with the observed intensity; the velocity differential in the HTZ is small and has therefore a small influence on the line profile. The latter is a double peak emission profile, even on central rays, with a central depression above the continuum level. The central depression is induced by the external border of the HTZ where a large amount of N V is generated, leading to a large optical depth for the central frequency of the line. On central rays, the double peak emission shape is only due to this influence, but for higher latitudes, the influence of the velocity field is getting stronger; two peaks are seen (in emission because formed on no background continuum), one produced by the part of the HTZ moving towards us, the other by the receding part of the HTZ. Their separation is a consequence of the large velocity gradient between the two emitting regions, larger than the line width. The resulting emergent flux profile is a double peak emission profile, very different from the observed profile. The temperature of the HTZ is now sufficiently high to deplete N IV, and no strong emission is produced for the N IV 1718.51 Å line. However, these models produce an intense emission component in

the C IV line, which is not observed (see Fig. 1). They must therefore be discarded.

As the HTZ moves farther away from the top of the chromosphere, its width and temperature have to increase to compensate for the decrease of the density. On central rays, the line now appears in absorption because of the large increase of column density. For high values of impact parameters, the two emission peaks are still present, and have the same origin as previously discussed. On the resulting emergent flux profile, a double peak emission profile with a central depression under the continuum level is obtained, which again is very different from the observed profile.

The more the HTZ moves away from the top of the chromosphere, the deeper the absorption on central rays. Furthermore, this absorption is more and more blueshifted, the macroscopic velocity field increasing outward. A P Cygni profile is eventually formed.

In summary, these spherically symmetric models fail to reproduce all of the observed line profiles at hand.

4.2. Models with corotating interaction regions

The main difficulty of the homogeneous models presented in the previous section is the production of N IV and/or C IV emission lines, which are not observed. However, this emission can be reduced until it becomes undetectable if the filling factor of the HTZ is small. Models with shocks producing hot clumps of material in the wind would lead to such small filling factors. We therefore considered models in which:

- fast and slow streams in the wind alternate on the line of sight as the star rotates,
- shocks occur where fast streams overtake the slow ones.

These assumptions are supported by several observations of the spectroscopic variability of AB Aur (Praderie et al. 1986, Catala et al. 1986, Simon et al. 1990, Böhm et al. 1996), showing a rotational modulation in Mg II resonance lines, the Ca II K 3933 Å line and the He I 5876 Å lines, which is likely to originate in the stream structure of the wind. The difference in velocity between the fast and the slow streams would be of the order of 100 km.s^{-1} (measured from the variation of the maximum blue-shift of the Mg II absorption component).

This model was inspired from the solar wind, in which fast and slow stream structures are controlled by the surface magnetic field. In the solar wind, a pair of shocks (one direct, one reverse) is formed where a fast stream overtakes a slow one, and a corotating interacting region (CIR) is observed between these two shocks. In the CIRs, the velocity is intermediate between that of fast and slow streams, while the density is enhanced and the temperature has a complex profile and can reach several million degrees (Burlaga 1984, Mullan 1984). Models of CIR have been proposed for various kinds of stellar winds (Mullan 1984), and more specifically for Herbig Ae/Be stars (Catala et al. 1986). The distance of the CIRs from the star's surface is primarily a function of V_{rot}/V_{exp}, where V_{rot} is the rotation velocity at the surface and V_{exp} the expansion velocity in the wind. While this ratio is very small in the solar case ($\approx 5 \times 10^{-3}$), it can be much higher in the case of AB Aur (≈ 0.2), and therefore the CIRs can be located close to the star's surface. Because the temperature in the CIRs is expected to rise far above that of the unperturbed stellar wind, we may assume that the N V resonance lines can originate in part of the CIRs, while X-ray emission is produced in the hottest parts of them.

In order to simulate the presence of such CIRs in the wind of AB Aur, we have introduced a very low velocity gradient throughout the HTZ, with values of the velocity of about 100 km.s^{-1}. Finally, we have assumed that the CIRs, modeled by the HTZ, occupy only a small fraction of the surface, represented by the filling factor *f*.

We can first derive constraints on the location of the CIRs and on the temperature in the region forming the N V lines, in the following way:

- The CIRs must be located above the minimum of temperature reached just after the photosphere, and cannot be located outside the chromosphere. Indeed, in this case, they would have to be so wide and their filling factor so large to compensate for the lower density that profiles of lines like Hα and Mg II 2795.5 Å would be deeply affected and would no longer match the observed profiles. Therefore, Δ_3 can only range from $0.003R_*$ to $1.4R_*$.
- The maximum temperature in the regions of the CIR forming the N V lines is in the range T_{min}=110,000K – T_{max}=160,000K, the former being the minimum value under which a significant N IV line appears for the models leading to a N V line as observed, the latter being that above which the intensity of the N V line begins to drop below the observed one, even with f = 1.

However, except for these straightforward constraints on the location and the temperatures of the CIRs, no more precise information can be obtained from the fitting of the line profiles alone, since it is always possible to find an ad hoc value of the filling factor f leading to a good fit of the observed profiles for any pair (Δ_3 ; T) in the range mentioned above.

The constraints can be refined if we now assume that the CIRs are also responsible for the X-ray emission of AB Aur. The amount of energy radiated by AB Aur in the spectral range [0.1-2.4 kev] is: $L_X \simeq 3.3\ 10^{29}$ ergs.s^{-1}, this figure being derived from ROSAT data (Zinnecker & Preibisch 1994). In this energy range, it is mainly due to thermal bremsstrahlung emission. In the framework of the CIR model, we can estimate the expected X-ray luminosity of AB Aur as

$$L_X = 16\pi^2 R_{htz}^2 \Delta R\, f \int_{\nu_1}^{\nu_2} \varepsilon_\nu^{\rm ff}\, e^{-\tau_\nu}\, d\nu \qquad (12)$$

Here, $\varepsilon_\nu^{\rm ff}$ is the power per unit volume and per unit frequency radiated at frequencies in the range $[\nu_1 - \nu_2]$ (corresponding to [0.1-2.4 kev]) by thermal bremsstrahlung, f is the filling factor of the CIRs introduced earlier, and τ_ν is the optical thickness of the regions of the wind surrounding the CIRs, calculated from the usual free-free absorption coefficient (see for example Rybicki & Lightman p162). The quantity $\varepsilon_\nu^{\rm ff}$ depends on the

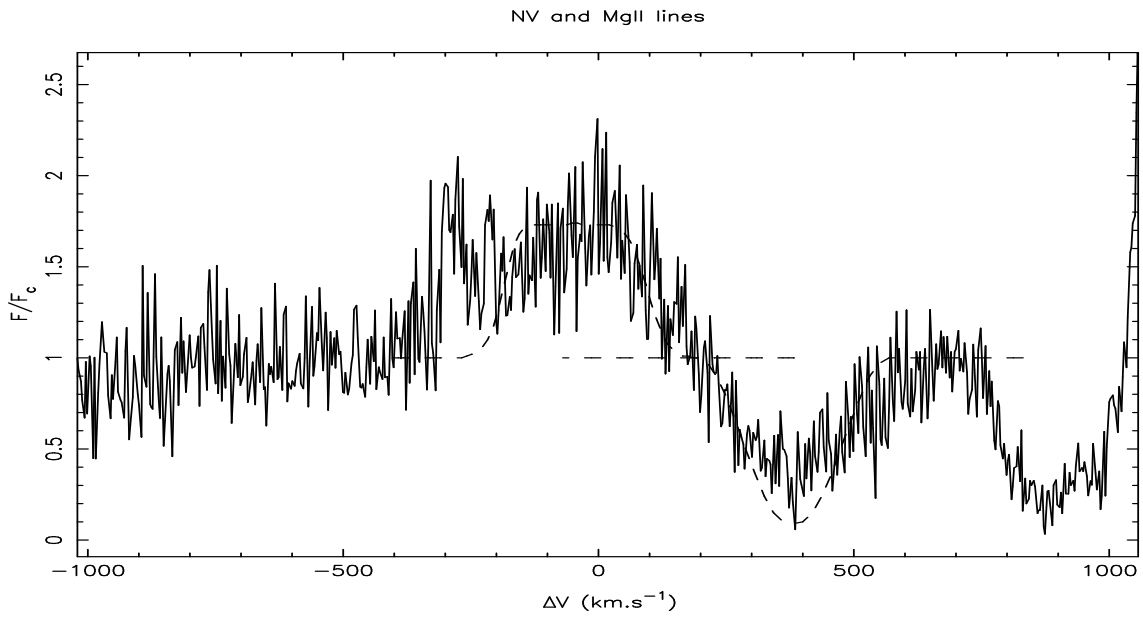

Fig. 5. N V line and Mg II line profiles computed with the "best fit model" (dashed lines), plotted over the observational spectrum.

Table 4. Parameters of the best fit model (R_{ph} = 1.75 × $10^{11} cm$ is the photospheric radius)

R_{ch}	T_{max}	T_0	Δ_3	Δ_4	T_{htz}	v_D	f
1.04 R_{ph}	17000 K	3000 K	0.05 R_{ph}	0.01 R_{ph}	140000 K	75 km.s^{-1}	7.e- 3

temperature reached in the plasma and on the product of the electron density n_e and the ion density n_i (see for example Rybicki & Lightman p160). We have also assumed a plasma maximum temperature in the CIRs of $T_{\rm CIR}$ = $10^7 K$, which is the value considered in Zinnecker & Preibisch study. Finally, we have assumed a Gaunt factor of unity.

The assumption that the CIRs are responsible for the observed soft X-ray emission of AB Aur thus gives us an additional relation between the location and the filling factor of the CIRs. We have performed a systematic exploration of the entire parameter space of our model, which provided us with a "best fit model", in agreement both with the spectroscopic constraints and the X-ray emission of AB Aur. Note that we have considered that the Doppler random velocity v_D was a free parameter of our model. This quantity represents small scale motions in the region of formation of the lines, and was estimated to be 45 km.s^{-1}, from the analysis of the hydrogen Balmer lines (CK). However, since we are now dealing with CIRs, where the physical conditions may be very different from those of the outer stellar wind where the hydrogen lines are formed, there is no reason to assume that v_D should have the same value as in CK. In practice, higher values for v_D than in CK are required to reproduce the correct width and shape of the observed N V line. We found v_D = 75 km.s^{-1} as the best value of this parameter. Table 4 list the values of the parameters of the best fit model.

Fig. 5 displays the synthetic profile of the N V line at 1238.8 Å obtained with our best fit model, together with the photospheric Mg II line at 1240.4 Å. One can readily check that a convincing fit of that part of the spectrum is obtained.The theoretical N V profile is rather more box-like or square, compared with the observed emission line, which suggests that the distribution of clump regions is not quite right, needing either more of them at zero velocity or else a higher circular velocity around the star to spread more of the emission into the wings. However, we feel that the present model yields a satisfactory fit of the observed N V intensity and profile, and that the derivation of a more complex and more sophisticated model is out of the scope of this study. We have also confirmed that this model reproduces correctly all of the other spectroscopic observations at hand: deep, wide, blueshifted absorption C IV resonance lines, identical to those obtained by Catala (1988), no emission for the N IV 1718.51 Å and 7651.4 Å lines, Mg II resonance lines with a type IV P Cygni profile, as in Catala et al. (1984), and hydrogen Balmer lines and continuum unchanged compared to the results of CK.

4.3. Radiative losses

In order to maintain the chromosphere of AB Aur, a large amount of nonradiative energy must be deposited in the wind, which can be estimated by the calculation of the radiative losses. We can use the mean radiation intensity and the source function

Table 5. Dominant contributors to the radiative losses

Transition	$E^-_{CIR}(ergs.s^{-1})$
Mg II $^2S - ^2P^o$	4.5 (+26)
C III $^1S - ^1P^o$	1.7 (+28)
C IV $^2S - ^2P^o$	2. (+30)
C III Cont.	5.4 (+28)
C IV Cont	9. (+28)
N IV $^1S - ^1P^o$	4.5 (+28)
N IV $^1P^o - ^1D$	2.8 (+27)
N V $^2S - ^2P^o$	4.8 (+30)
N IV Cont.	1. (+29)
N V Cont.	7.6 (+29)
Hα	4.9 (+26)
Hβ	3.8 (+26)
Hγ	2.4 (+26)
Hδ	2.3 (+26)
Pβ	1.1 (+26)
Pγ	1.5 (+26)
Lyman Cont.	1.3 (+29)
Balmer Cont.	5.2 (+28)
Paschen Cont.	1.4 (+28)
Brackett Cont.	7. (+27)
Pfund Cont.	3.9 (+27)
Humphrey Cont.	2.5 (+27)
X $[0.1 - 2.4kev]$	3.3 (+29)
Total	8.3 (+30)

of each transition we have calculated to evaluate its contribution to the radiative losses in each point of the wind:

$$E^-(r) = 4\pi \int_0^\infty \chi_\nu (S_\nu - J_\nu) d\nu \quad (\mathrm{ergs.cm^{-3}.s^{-1}}) \qquad (13)$$

Note that E^- is positive when the medium cools by radiation. Earlier calculations have shown that the radiative losses in the chromosphere of AB Aur are very large (6% of the star's luminosity) and mostly dominated by the Balmer continuum (Catala 1989). It is now necessary to estimate the additional radiative losses induced by the CIRs. To this end, we have used our computations of the various lines and continua (from hydrogen, magnesium, carbon and nitrogen) to calculate their contributions to E^-, then integrated $E^-(r)$ over the region affected by the CIRs. The result of these computations is that both the C IV line and N V line now dominate the radiative losses in the regions of the CIRs producing the N V resonance lines. As far as continua are concerned, continuum from N V and the Lyman continuum are the dominant radiators in this region. In the hottest parts of the CIRs, assumed to be at 10^7 K, the radiative losses are dominated by X-ray emission.

Table 5 shows the various contributions to the radiative losses in the CIR which are 8.3×10^{30} ergs.s^{-1}.

The radiative losses evaluated with the old model without the high temperature zone are about 4×10^{34} ergs.s^{-1}. We therefore conclude that the presence of CIRs keeps the global energetic balance of the wind of AB Aur almost unchanged. However, the flux of energy that must be dissipated in the CIRs to account for the radiative losses exceeds by more than one order of magnitude the flux of kinetic energy across the CIRs, which we have calculated assuming a mass loss rate of 1.1×10^{-8} M$_\odot$yr^{-1}, and a velocity difference between the fast and slow streams of 100 kms^{-1}. This shows that other processes than dissipation of kinetic energy in the CIRs must be present. The shocks at the boundaries of the CIRs are very likely to be MHD shocks, in which mechanisms like dissipation of Alfvèn waves or Ohmic heating must take place. Assuming a magnetic field intensity of about 100 G, which corresponds to the equipartition field at the stellar surface (Catala et al. 1993), we find that the magnetic energy flux across the CIRs is several orders of magnitude above their radiative losses, so that the magnetic field constitutes a comfortable reservoir of energy to account for the observed phenomena.

5. Conclusion

Observations by HST have revealed the presence of N V in the wind of AB Aur, which indicates that layers exist in the wind of this star with higher temperatures than those previously deduced from observations and modelling of several spectral lines.

A full computation of the N IV–N V–N VI system has been performed to study the formation of the lines of these species in the wind of AB Aur. Models including a spherically symmetric high temperature zone in addition to the usual chromosphere can reproduce the observed N V line, but also produce strong emission lines for N IV and C IV, which are not observed. On the other hand, models including discrete hot regions, such as expected if corotating interaction regions are present in the wind, successfully reproduce the observed spectroscopic features, as well as the X-ray flux of AB Aur as observed by ROSAT.

Temperatures of the order of 140,000 K are necessary to produce the observed N V line, while temperatures in excess of 10^6 K are required to explain the X-ray flux. The width of the CIRs must be of about $2 \times 10^{-2} R_*$, i.e., 3.5×10^9 cm, while their surface geometrical filling factor is 7×10^{-3}. The radiative losses in the CIRs reach about 8.3×10^{30} erg.s^{-1}, which is negligible compared to the total radiative losses of the chromosphere.

Clearly these new observations provide another clue that the wind of AB Aur is very inhomogeneous and includes azimuthal structures giving rise to corotating interaction regions. Further studies of these structures would be of utmost interest. In particular, all features produced in the CIR, such as the N V lines, or X-ray flux, are expected to be variable, and the study of their variability would bring us valuable information on the structure of AB Aur's wind.

Furthermore, the recent discovery of a surface magnetic field for the Herbig Ae star HD 104237 (Donati et al. 1997) gives an additional credit to the hypothesis we are defending here. New attempts for direct detections of magnetic fields in Herbig Ae/Be stars should be performed in the future.

Acknowledgements. T.S. gratefully acknowledges the support of NASA grant GO-6071.01-94 from the Space Telescope Science Institute, which is operated by the Association of Universities for Research in Astronomy, Inc., under NASA contract NAS5-26555. We thank Dr.

I. Hubeny for valuable discussions, and for putting his TLUSTY code at our disposal.

References

Artru M.-C., Borsenberger J., Lanz T. 1989 A&AS, 80, 17
Böhm T., Catala C. 1993 A&AS, 101, 629
Böhm T., Catala C. 1994 A&A, 290, 167
Böhm T., Catala C., Carter B., Baudrand J., Butler J., Collier-Cameron A., Czarny J., Donati J.-F., Foing B.H., Ghosh K.K., Houdebine E., Huang L., Jiang S., Hao J., Neff J., Rees D., Semel M., Simon T., Talavera A., Welty A., Zhai D., Zhao F. 1996, A&AS, 120, 431
Burlaga L.F., 1984, Space Science Review, 39. 255
Catala C., Praderie F. & Kunasz, P.B. , 1984, A&A, 134
Catala C., Felenbok P., Czarny J., Talavera A., Boesgaard A.-M., 1986, ApJ 308, 791
Catala C., Kunasz P.B. 1987, A&A 174, 158
Catala C., Praderie F., Felenbok P., 1987, A&A, 182, 115
Catala C., 1988, A&A, 193, 222
Catala C. 1989, in *Modeling the Stellar Environment: How and Why?*, 4th IAP meeting, Paris, eds: Ph. Delache, S. Laloe, C. Magnan, J. Tran Thanh Van, p. 207
Catala C., Böhm T., Donati J.-F., Semel M. 1993b, A&A, 278, 187
Catala C., Böhm T., Donati J.-F., et al. 1994, Solar Phys., 155, 185
Donati J.-F., et al. MNRAS (*in press)*
Finkenzeller U., Jankovics I., 1984, A&AS, 57, 285
Finkenzeller U., Mundt R., 1984, A&AS, 55, 109
Hidalgo M.B., 1968, ApJ, 153, 981
Kelly R.L., Palumbo L.J., 1973, *Atomic and Ionic Emission Lines Below 2000* Å NRL Rep.7599
Kurucz R.L., 1979, ApJS, 40, 1
Mihalas D., in *Stellar Atmospheres*, 2nd edition
Mihalas D., Kunasz P., 1978, ApJ, 219, 635
Mullan D., 1984, ApJ, 283, 303
Peach G., 1967, *Mem* R.A.S, 71, 1
Praderie F., Simon T., Catala C., & Boesgaard A.M. 1986 Ap.J., 303, 311
Rybicki G., Lightman A., in *Radiative Processes in Astrophysics*
Sahal-Brechot S., Segre R.A., 1971, A&A, 13, 161
Seaton M., 1962, in *Atomic and molecular processes*, ed. D. R. Bates (New-York; Academic Press), p. 374
Simon T., Catala C. & Praderie F.: 1990, in *Cool stars, Stellar systems and the Sun* (Springer-Verlag)
Soderblom, D. R., Gonnella, A., Hulbert, S. J., Leitherer, C., Schultz, A., & Sherbert, L. E. 1995, *Instrument Handbook for the Goddard High Resolution Spectrograph (GHRS)*, Version 6.0 (Baltimore, MD: Space Telescope Science Institute.
Strom S.E., Strom K.M., Yost J., Carrasco L., Grasdalen G.L., 1972, ApJ, 173, 353
Van Regemorter H., 1962, ApJ, 136, 906
Zinnecker H., Preibisch Th., 1994 A&A 292, 152

This article was processed by the author using Springer-Verlag LaTeX A&A style file *L-AA* version 3.